Sensors & Actuators: B. Chemical 274 (2018) 616–626

Contents lists available at ScienceDirect

Sensors and Actuators B: Chemical

journal homepage: www.elsevier.com/locate/snb

Polyaniline nanocomposites based sensor array for breath ammonia analysis. Portable e-nose approach to non-invasive diagnosis of chronic kidney disease

Paul Le Maout[a,*], Jean-Luc Wojkiewicz[b], Nathalie Redon[b], Cyril Lahuec[a], Fabrice Seguin[a], Laurent Dupont[a], Sergei Mikhaylov[c], Yuriy Noskov[c], Nikolay Ogurtsov[c], Alexander Pud[c]

[a] IMT Atlantique, ELEC Department, Technopôle Brest-Iroise CS83818, 29238 Brest, France
[b] IMT Lille-Douai, Univ. Lille, SAGE-Department, Sciences de l'Atmosphère et Génie de l'Environnement, F-59000 Lille, France
[c] Institute of Bioorganic Chemistry and Petrochemistry, National Academy of Science of Ukraine, Ukraine

ARTICLE INFO

Keywords:
Polyaniline nanocomposites
Sensor array
Breath analysis
Ammonia
Classification
Chronic kidney disease diagnostics

ABSTRACT

Kidney failure is a serious chronic disease, defined as the irreversible loss of kidney function. This disease is clinically silent to a very advanced stage. Thus, only a screening procedure can diagnose its pathology early enough to slow its progression. Due to the known fact that pathology of this disease is characterized by an increase of ammonia concentration in breath, its monitoring with a portable system can be a simple way for a noninvasive and early diagnostic on site. To realize such a system a new specific conductometric array of 11 different polyaniline nanocomposite sensors is used, based on the electronic nose principles. This approach allows bypass sensor weaknesses (sensor drift and sensitivity to humidity) and to determine ammonia in the typical concentration range of human breath (500 ppb–2100 ppb). In particular, polyaniline based nanocomposites with either titanium dioxide, chitosan or carbon nanotubes are used to provide different sensitivities and response times. This allows associating a single pattern of sensor responses to a concentration range. Maximum variation of resistance, derivative and integral values are extracted from the response curves of each sensor. Common classifiers are then tested and a selection feature algorithm is used. It permits improving the measurement accuracy and determining the most relevant features and sensors. Diagnosis accuracy reaches 91% with the combination of feature selection and Support Vector Machine algorithm.

1. Introduction

Human breath is a complexenvironment with a high relative humidity, above 90% and with several hundreds of compounds. Their concentrations range from few ppt up to thousands of ppm [1,2]. Moreover the variability of the composition is important between individuals and depends on many factors such as age, gender or health condition. Over the last decade, a correlation between diseases and gas compounds present in the breath has been studied [3–5]. In particular, for hepatic or kidney disease, ammonia has been noted as one of the relevant markers [6]. This compound is a breakdown product of proteins which is usually transform into urea by the liver and evacuated through the kidneys. When one of these two organs fails, the ammonia concentration increases from few hundred ppb when healthy up to several ppm [7]. In this study, a concentration up to 1.1 ppm of ammonia is considered healthy, while beyond 1.6 ppm as unhealthy [8]. Since the boundary between healthy and unhealthy is fuzzy, an intermediate concentration range is defined.

With 5% of the global population affected by chronic kidney disease [9], the development of a non-invasive, easy to use and cost-effective solution to diagnose kidney pathologies is of utmost importance. In order to check patients for kidney diseases two tests are currently in use: a blood and a urine tests. The first one assesses the glomerular filtration rate while the second one the abnormal presence of proteins. Both these procedures are simple and cost-effective but require specific an operator and a laboratory. Moreover, blood tests are invasive.

Being able to detect and quantify ammonia at an early stage with a non-invasive tool that is easily accessible to the general practitioner would improve the diagnosis and thus the prospects of an effective treatment. Measuring the concentration of ammonia in patient breath is then a promising approach. The accuracy of the measuring system is then crucial to minimize diagnosis errors. A limit of detection of at least

* Corresponding author at: IMT Atlantique, ELEC department, Technopôle Brest-Iroise CS 83818, 29238 Brest, France.
E-mail addresses: paul.lemaout@imt-atlantique.fr (P. Le Maout), jean-luc.wojkiewicz@imt-lille-douai.fr (J.-L. Wojkiewicz), alexander.pud@bpci.kiev.ua (A. Pud).

https://doi.org/10.1016/j.snb.2018.07.178
Received 18 April 2018; Received in revised form 2 July 2018; Accepted 31 July 2018
Available online 02 August 2018
0925-4005/ © 2018 Elsevier B.V. All rights reserved.

500 ppb and a measurement accuracy of less than 100 ppb are chosen in this study to comply with the concentrations ranges defined above.

This could be achieved with standard analytical measuring tools. However these systems are expensive, bulky and hard to use. Therefore, they could not allow a broader access to point of care testing [10]. For example, reference measurement systems based on Cavity Ring Down Spectroscopy technique, such as LGR Ammonia Analyzer, cost thousands of dollars and weights over 30 kg. Gas Chromatography and Mass-Spectrometry (GC–MS) methods, which are also widely used in breath testing, have similar constraints.

In order to achieve an economically viable system to be distributed to general practitioners, an autonomous, portable and easy-to-use measurement system based on single gas sensor or gas sensor array is a promising solution [11,12]. Nevertheless, there are limitations related to non-specificity, limit of detection, response time and sensitivity to humidity that need to be addressed.

Several techniques are currently being investigated such as Quartz Crystal Microbalance (QMB) [13]. A functionalized material sensitive to ammonia is deposited on a quartz crystal. When exposed to ammonia, the coated quartz mass changes. In particular, Kikuchi et al. developed a QMB ammonia sensor which was capable of measuring 1 ppm of ammonia. However, this limit of detection is too high to comply with the specifications of the application [14]. Conductivity variation, or equivalently, complex impedance variation is another mechanism used for several types of gas sensors [15]. Gouma et al. developed a metal oxide (MOX) sensor based on a semi-conducting ceramic, MoO3 [16] whose detection limit is below 50 ppb. The major disadvantage of MOX sensor materials is, however their high energy consumption due to the need to heat them at high temperature, around 500 °C. This would impact the autonomy of a portable system [15]. Sensors based on intrinsically conductive polymers such as polyaniline (PANI) are sufficiently stable, fast and sensitive with acceptable detection limit at ambient temperatures due to the reversible changes in their conductivity [17]. While conductivity of polyaniline and its nanocomposites materials depend on various factors, for ammonia sensing the most important factor is obviously its protonation (doping) degree by an acid-dopant. In particular, when exposed to ammonia, polyaniline is deprotonated leading to a decrease in its conductivity [18]. However, polyaniline based sensors still have some limitations. Thus, the response variability and the influence of humidity must be counteracted and the response time must be accelerated. Mérian et al. have made a composite of polyaniline and polyurethane that lowers the limit of detection down to 7 ppb [19]. To get synergetic effects between the components, hybrid polyaniline nanocomposites were intensively investigated and particularly in the field of gas sensors [20]. Mikhaylov et al studied a core shell system where PANI coats the TiO2 particle, giving a high surface/volume ratio [18,21]. The latter provides a very low detection limit of about 50 ppt [19]. This sensor must therefore be protected from light sources to avoid degradation. The complete synthesis process and characterization is described in [18].

In the same way, it has been suggested that the electrical properties of the CNT/PANI composites are improved compared to the raw polyaniline due to the charge transfer from the conducting polymer to the CNT through a π-π aromatic interaction. The charge localization and probably the hopping distance were found to be decreased with the percentage of CNT (wt) in the nanocomposites. While the charge hopping energy was found to be decreased in nanocomposites [22–24].These properties are used to elaborate efficient chemical sensors [23,24]. In a concentration range of ammonia of 0.2 to 15 ppm, He et al., showed a linear response for a sensor based on CNTs and polyaniline [25].

These examples show the efficiency of PANI and its nanocomposites to detect ammonia even at very low concentrations (ppb). Nevertheless, their application in a human breath medium has not been fully investigated. Hibbard et al. developed an inkjet-printed polyaniline sensor to measure the concentration of ammonia in a simulated human breath. However, the sensor has to be exposed during ten minutes to discriminate efficiently the different concentrations [25]. Santos et al. used impedance spectroscopy to measure the real and the imaginary parts of the complex impedance of a thin film polyaniline sensor. Although the measurement accuracy is greater than 95% for a 1 min exposure time, the study was conducted in too high concentration ranges, from 9 ppm to 20 ppm [26].

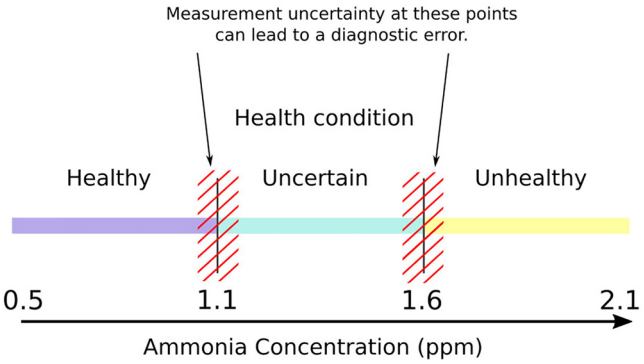

Fig. 1. Ammonia concentration ranges and corresponding health condition. Sensor sensibility is particularly important to correctly diagnose.

Finally, all these studies used only one single sensor. The problems of sensor fault, drift or repeatability due to manufacturing variations therefore arise. The last two can yield a different diagnosis when the ammonia concentration lies at the limit between two diagnosis ranges, Fig. 1.

To overcome these problems and to meet the specifications of the application, the proposed solution is to use the electronic nose principles [27]. These principles associate a single fingerprint of sensor responses with a concentration range by using a classification algorithm. Sensors must therefore have differentiated responses. It becomes possible to reduce drift, aberrant values while maintaining the diagnostic accuracy [28]. Polyaniline is chosen to form the sensitive base material for the sensor array because it provides many advantages such as low cost, high sensitivity to ammonia and applicability in different nanocomposite formulations with e.g. semiconducting inorganic nanoparticles, polymers etc. to have differentiated responses [29]. The last option facilitates both an enhancement of polyaniline sensitivity for account of the specific surface increase and an improvement of its selectivity due to physical-chemical interactions along the interfaces of polyaniline with other component of the nanocomposite responses [30]. Taking into account the above discussion, this work presents:

- Polyaniline nanocomposite based sensors that combine sensitive surfaces/interfaces of different chemical formulations with different sensitivities and metrological performances.
- Extraction of features which are still unexploited, especially those characterizing the response dynamics.
- A first algorithm that permits to select the best subset of features and a second algorithm that gives the best diagnostic accuracy.

The idea is to find the best combination of the polyaniline compositions to be used, the best features and the best classification algorithm. The rest of this paper is organized as follows: the first part tackles the fabrication of the sensors and the sensing system. The second part deals with the extraction of the features and algorithms used. The last part is about the results and conclusion.

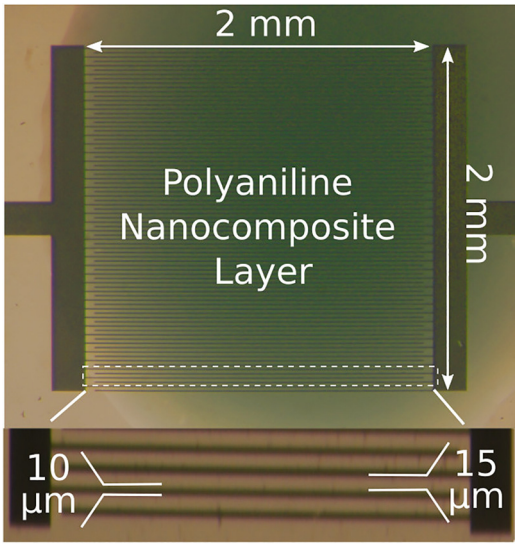

Fig. 2. Picture of one of the prepared sensor showing a polyaniline nanocomposite layer on interdigitated electrodes.

2. Experimental

2.1. Polyaniline nanocomposites preparation and morphology characterization

Building the electronic nose necessitates fabricating sensors with different sensitivities and response times. Each sensor consists of a polyaniline based formulation deposited on chrome/gold interdigitated electrodes. The latter are made with photolithography on a glass substrate. The area of the interdigitated electrodes is 2 × 2 mm, the inter-electrode space is 15 µm and the width of the electrode is 10 µm, Fig. 2.

The first type of polyaniline formulations is its nanocomposites with a non-toxic and stable biopolymer chitosan (chitosan 95/1000 Heppe Medical, Germany [31]). This nanocomposite is prepared by co-dissolution of the components at different weight ratios in accord with the protocol described in [32]. In short, emeraldine base doped with camphor sulfonic acid and chitosan were dissolved separately in lactic acid. After total dissolution the two components were mixed under stirring with appropriate quantities (see Table 1, 20%, 50% and 75% indicate that the composites contain respectively 20%, 50% and 75% of doped PANI in mass). The solution was mixed for few days and then sonicated for two hours. A homogenous clear green solution was obtained for deposition on electrodes.

The second one is presented here by the core-shell nanocomposites based on the semi-conducting metal oxide namely titanium dioxide TiO_2 5–10 nm nanoparticles (anatase form, MTI Corporation). These nanocomposites had the core-shell morphology due to the fact that they were prepared by the same oxidative aniline polymerization protocol as in [18]. Shortly, the preparation involved aniline (Merck) polymerization in the presence of the acid-dopant dodecylbenzenesulfonic acid (DBSA, Acros) and TiO_2 nanoparticles dispersed in the reaction medium at 10 °C under the action of ammonium persulfate (APS, Ukraine). Different contents of polyaniline in the nanocomposites were predetermined containing 8.7%, 18.9%, 36.1% and 79.2% of doped PANI in mass. These nanocomposites after the polymerization procedure were dialyzed against distilled water for 72 h and dried under vacuum at 60 °C to a constant weight.

The third type of the prepared formulations includes nanocomposites of multi-wall carbon nanotubes (CNTs) and polyaniline doped with DBSA. These CNT/PANI nanocomposites were synthesized precisely in accord with the protocol described in [18]. It has been performed through oxidative chemical aniline polymerization using oxidant $(NH_4)_2S_2O_8$ in a presence of CNT and DBSA in the reaction water medium with initial MWCNT/aniline weight ratios concentrations of 80/20, 40/60 and 30/70. This procedure resulted in formation of the core-shell nanocomposites containing 40.5 wt.%, 80.3 wt.% and 86.4 wt.% of PANI doped with DBSA, respectively. Complete characterization of these nanocomposites is given in [33]. By previous tests the CNT/PANI nanocomposite with the intermediate PANI-DBSA loading 80.3 wt.% was chosen for the sensing measurements while samples with 40.5 wt.% and 86.4 wt.% of PANI doped by DBSA were excluded.

Transmission electron microscopy (TEM) images of Chitosan/PANI nanocomposite, TiO_2/PANI and CNT/PANI nanocomposites were obtained with FEI Tecnai G2-20 Twin High resolution and JEOL JEM-1400. Scanning electron microscopy (SEM) images of Chitosan/PANI nanocomposite, TiO_2/PANI and CNT/PANI nanocomposites were obtained with HITACHI S-4300 SEM and JEOL JSM-6060 LV microscopes

2.2. Sensors fabrication

The synthesized polyaniline containing nanocomposites were dispersed in dichlorobenzene for TiO_2/PANI and CNT/PANI nanocomposites while Chitosan/PANI composites are in the form of solution as described previously. In both cases the operations were performed at room temperature. After sonication, each formulation was deposited by drop coating on the interdigitated electrodes and dried for 48 h at 80 °C.

A sensor array consisting of 11 sensors was fabricated (Table 1). Most electronic nose studies reduce their initial number of sensors to only a few to improve the measurement accuracy [34]. Eleven sensors are thus large enough to comply with the study specifications. In this array sensors 8, 10 and 11 have the same composition TiO_2/PANI (79.2 wt.%). It was repeated three times to study the impact of sensor redundancy in the electronic nose (Table 1).

2.3. Sensing system

Fig. 3 shows the system used to test the sensor array placed in a Teflon exposure chamber enclosed in a climatic chamber. The temperature is set at human breath temperature, 37 °C.

Gas mixtures are made using flow controllers in order to control the flow velocity, the humidity and the ammonia concentration. The sensors are exposed to a mixture of ammonia and moisture at 5 $L.min^{-1}$ flow rates. An LGR ammonia analyzer measures the concentration inside the exposure chamber in real time. Each injection of mixture of humidity and ammonia lasts one minute. Desorption lasts as long as exposition duration. The ammonia concentration in the mixture varies from 500 ppb to 2.1 ppm by step of 100 ppb. Relative humidity is 55% during exposition and 40% during desorption. The variations of the sensor resistances are measured with a digital multimeter (Agilent 34,970 A). Having a sufficient number of samples is essential to build a strong model. Hence, seven cycles of 51 injections of different concentrations of ammonia are done.

Table 1
Composition of the nanocomposites used in the sensor array.

Sensor number	1	2	3	4	5	6	7	8	9	10	11
Composite	Chit	Chit	TiO2	TiO2	CNT	Chit	Chit	TiO2	TiO2	TiO2	TiO2
Part of doped PANI (wt.%)	20	50	8.7	36.1	80.3	75	100	79.2	18.9	79.2	79.2

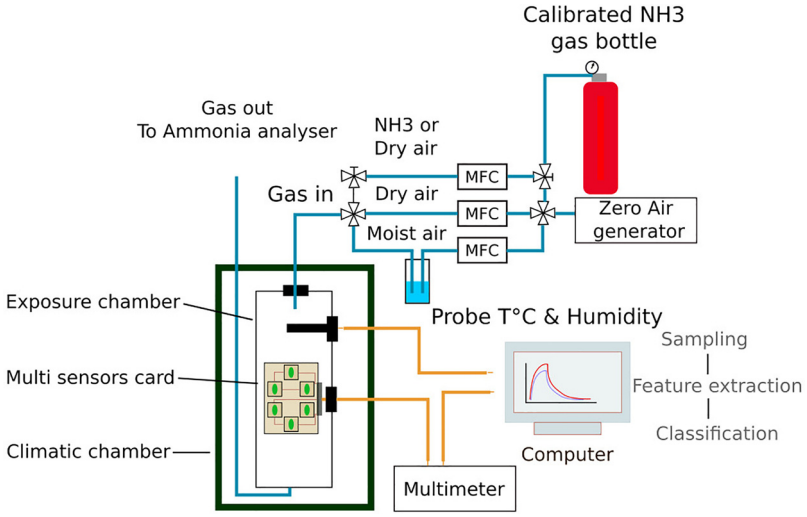

Fig. 3. Illustration of the sensor array test bench. A Mass Flow Controller (MFC) controls the individual mixing channels to the exposure chamber.

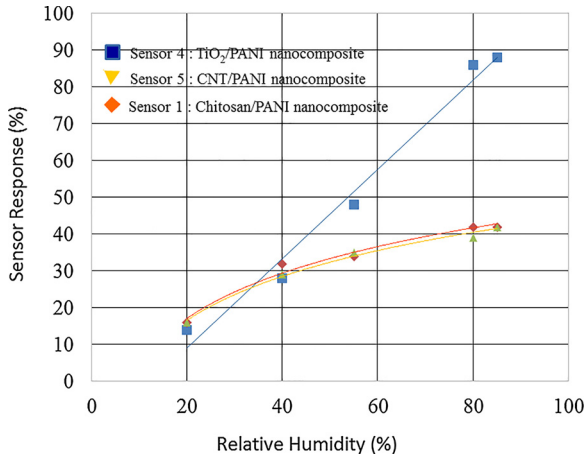

Fig. 4. Sensor response comparison of Chitosan/PANI, TiO2/PANI and CNT/PANI nanocomposite sensors to 1 ppm of ammonia at different humidity after 5 min of exposition.

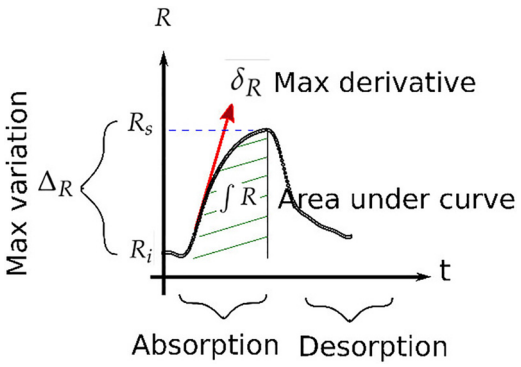

Fig. 5. Time variation of the resistive part of the sensor when exposed to ammonia and humidity first and then to air zero. Features are extracted during absorption and desorption.

While the used relative humidity values of 55% is lower than humidity in breath (typically 85%–95%), the influence of humidity in these sensors has previously been studied [18,35] and is also shown in Fig. 4. This Fig. 4 demonstrates the sensor response variation at 1 ppm of ammonia at different humidity levels after 5 min of exposure. Specifically, TiO_2-PANI nanocomposite shows the linear growth of the response in the humidity range 20–85 % to 1 ppm of ammonia while the two other ones are much less sensitive to the humidity changes and display tendency to a saturation. Nevertheless, despite some differences, the sensor responses at 5th min are increased by humidity in the same direction that will be taken into account during next studies, the responses monotonously increase, and the relative variation is unchanged, Fig. 4.

2.4. Features extraction

When the sensors are exposed to ammonia and humidity, a variation of resistance is measured, Fig. 5. Most research is only concerned with the maximum relative variation defined as:

$$\Delta R = \frac{Rs - Ri}{Ri} \quad (1)$$

Where *Rs* is the resistance at steady state, or maximum, and *Ri* at initial state. As the resistance of these sensors can increase during a few hours, or even days before saturation when exposed to ammonia, other features characterizing the responses dynamics must be extracted. In this study, two other features are thus selected, maximum derivative and integral value:

$$\int R = \int R(t)dt \quad (2)$$

$$\partial R = MAX\left(\frac{\partial R}{\partial t}\right) \quad (3)$$

All features are extracted during the absorption and desorption phases to double the number features used for classification. Once the features are extracted, it is necessary to find the best subset of features since it improves the classification accuracy. Among all these features, there is a redundancy of information. This helps identifying which sensors and features extracted from the curves are the most relevant, thus enabling optimization of future sensor arrays [36].

2.5. Feature and sensor selection

With *n*, the number of features, 2^n-1 training calculations are necessary to make an exhaustive search of the best subset. As *n* is 66 in this study, it is unrealistic to find an optimal subset of features. Fig. 6 shows how the features are then selected with the Recursive Feature Elimination algorithm. Beginning with all available features, the accuracy for a given classifier is calculated. A given classifier is tested with cross-validation, 60% of the dataset for the training phase, and 40% for the validation. The tested classifier allocates to each feature a

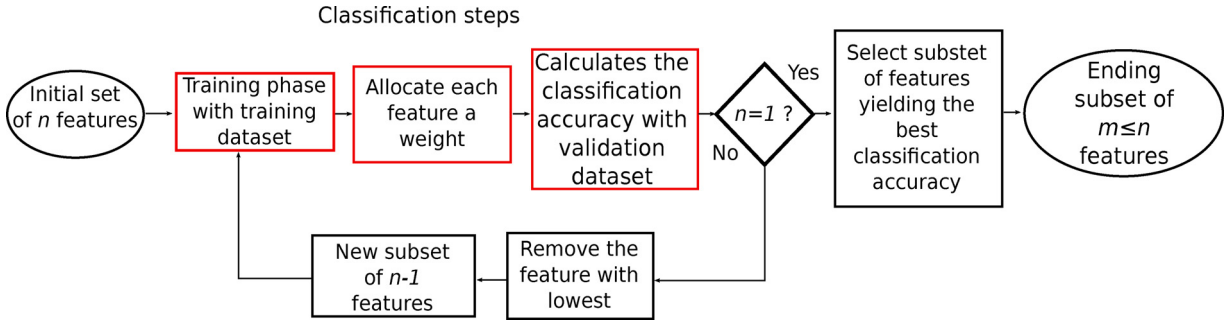

Fig. 6. Description of the Recursive Feature Elimination algorithm.

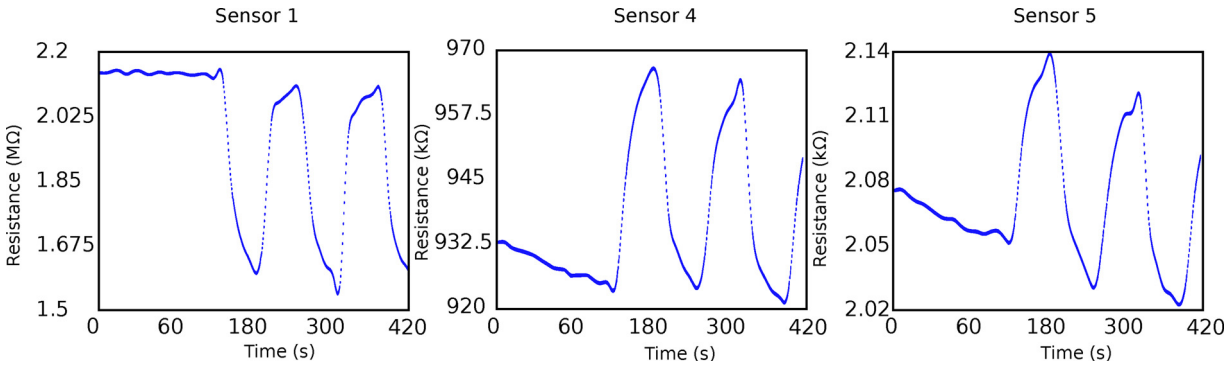

Fig. 7. Resistance variation of (a) chitosan/PANI nanocomposite sensor, (b)TiO_2/PANI nanocomposite sensor and (c)CNT/PANI nanocomposite sensor when exposed to 500 ppb and 600 ppb of ammonia.

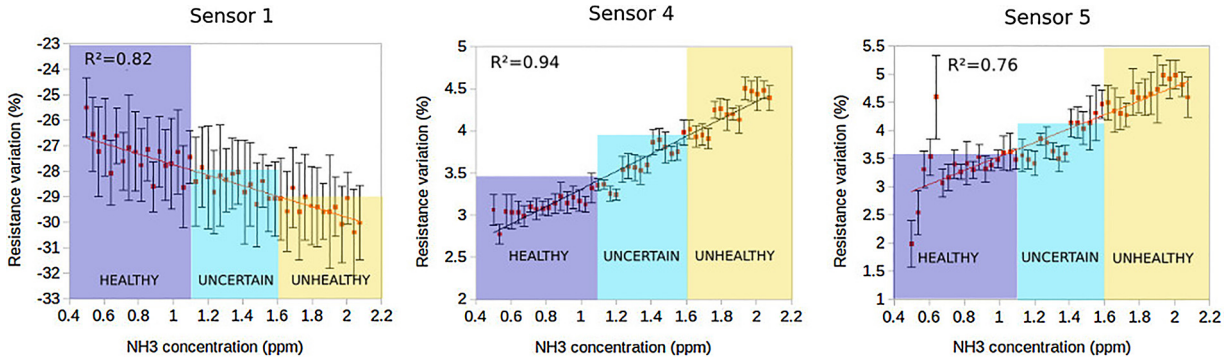

Fig. 8. Evolution of the resistance variation versus ammonia concentration for (a) sensor 1, based on chitosan/PANI, (b) sensor 4 based on TiO_2/PANI and (c) sensor 5 based on CNT/PANI.

weight. This weight allocation depends on rules specific to each classifier. The feature with the lowest weight is then eliminated. This operation is repeated until only one feature remains. The last step consists in selecting the subset of features with the best classification accuracy. The number of training calculations is reduced to n and the number of features to n or less. Common classification algorithms are tested: Discriminant Analysis (LDA), Random Forest (RF), Support Vector Machine (SVM) and Multi-Layer Perceptron (MLP).

LDA and SVM are both statistical methods. The principle of the first one is to find a linear combination of the inputs that maximizes the between-class scatter and minimizes the within-class scatter. LDA is the most used classification method [37] and is useful to visualize and interpret the result with a graphical display. Nevertheless, LDA can discriminate only classes that are linearly separable. On the contrary, SVM algorithm can cope with non-linear problems with the so-called "kernel trick" [38]. The latter idea is to find a new dimension space where the data become linearly separable. SVM is an efficient algorithm for high dimension data but it is sensitive to overfitting. The last two algorithms are not statistical methods because the output model depends on the initial state and the initial dataset and different parameters chosen for the learning phase. MLP is an artificial neural network, with an input and output layer and one or more hidden layers. A neuron is activated when the combination of the weighted inputs in the activated function passes a threshold. The output of the neuron is then propagated to the other neurons of the next layer until the output layer is reached. Finally, RF is based on multiple-decision tree classifiers. Each tree is built with a different data subset [39]. At each node of the tree, a parameter is compared to a threshold. This comparison decides which direction is taken in the tree until the leaf, which corresponds to the class, is reached. Only one leaf is then activated per tree. The result is calculated by counting the activated leaves on each tree. Scikit-learn libraries have been used to test these different algorithms [40].

3. Results and discussion

3.1. Sensing properties

In this subsection, the responses of 3 of the 11 sensors,

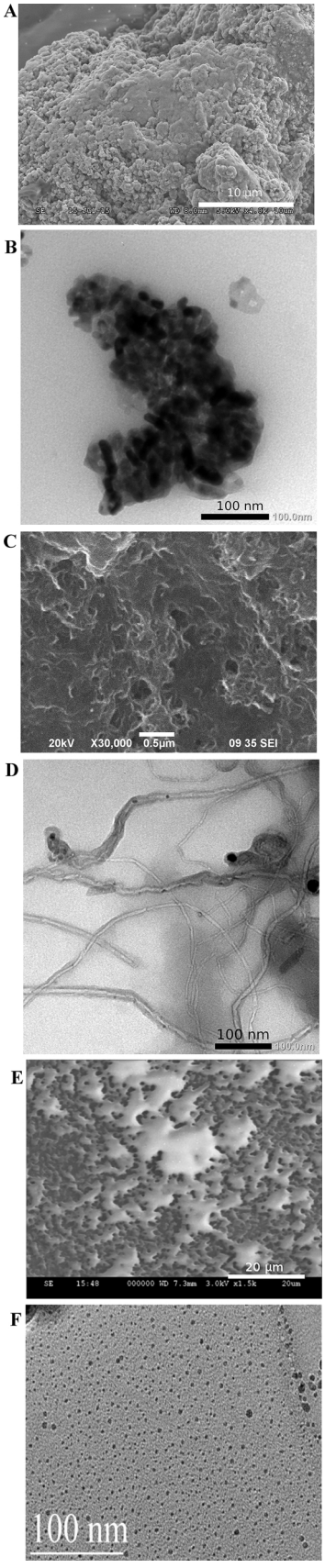

Fig. 9. (a) SEM and (b) TEM image of TiO2 /PANI nanocomposite. (c) SEM and (d) TEM image of CNT/PANI nanocomposite. (e) SEM and (f) TEM image of Chitosan/PANI nanocomposite.

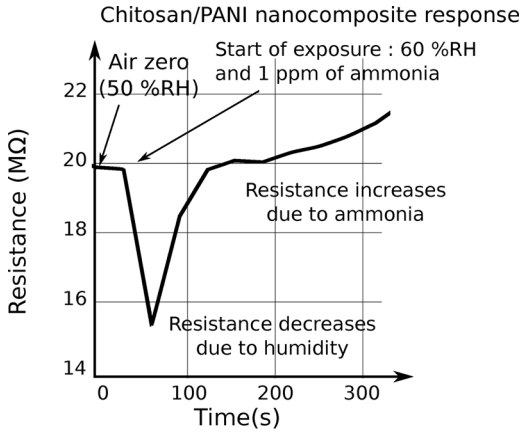

Fig. 10. Resistance variation of chitosan/PANI nanocomposite when exposed to a sudden increase of humidity from 50%RH to 60%RH and 1 ppm of ammonia. Time response is longer for ammonia than for humidity.

Table 2
Sensing specifications of the synthesized nanocomposite sensors.

Sensor	*Response sensitivity*	*Response time*	*Sensitivity to humidity*
Sensor 1: Chitosan/PANI nanocomposite	*0.12% / 100 ppb*	*> 1 min*	*Sensitive (non-linear)*
Sensor 4: TiO_2/PANI nanocomposite	*0.10% / 100 ppb*	*< 1 min*	*Sensitive (linear)*
Sensor 5: CNT/PANI-nanocomposite	*0.15% / 100 ppb*	*< 1min*	*Sensitive (non-linear)*

corresponding to each type of the formulated polyaniline nanocomposites are discussed. Fig. 7 shows the resistance transition curves of a chitosan/PANI nanocomposite sensor (sensor 1), TiO_2/PANI nanocomposite sensor and PANI/CNT nanocomposite sensor (sensor 4 and 5). The resistance decreases for chitosan nanocomposite and increases for CNT and TiO_2 nanocomposites when exposed to 500 ppb and 600 ppb of ammonia.

Fig. 8 shows the maximum variation of the resistance with ammonia concentration for sensor 1, based on chitosan/polyaniline nanocomposite, sensor 4 based on TiO_2/polyaniline nanocomposite and sensor 5 based on CNT/polyaniline nanocomposites.

In particular, chitosan/PANI sensor have a much higher relative resistance variation in the frames of around -30% compared to TiO_2/PANI or CNT/PANI sensors with dispersion of around 3%. The possible explanation of these different responses is that the chitosan/polyaniline composite (sensor 1) is prepared by mixing and forms a quite homogeneous and dense film at electrodes of transducer. In this film, most clusters of the sensitive polyaniline are embedded in the insulating chitosan matrix. Obviously, these clusters are located at different depths in the chitosan matrix and can work not as an ensemble but as separate particles giving their resistive responses modulated with a quite high level of the noise current. Unlike this, in case of the TiO_2/PANI (sensor 4) and CNT/PANI (sensor 5) core-shell nanocomposites porous layers are formed of the nanocomposite particles where the sensitive polyaniline is located completely on the surface of these overlapped nanoparticles with much better electrical contacts. Therefore, in the hybrid nanocomposites PANI is directly opened to the analyte. This explanation matches well with SEM and TEM images of the nanocomposites. Specifically, TiO_2/PANI and CNT/PANI nanocomposites (Fig. 9b, d) confirm the core-shell structure, which both is formed by TiO_2 (or CNT) with PANI and gives a high surface/volume ratio.

As it is shown in the SEM images (Fig. 9a,c and e), the chitosan/PANI morphology presents a smoother surface than two other

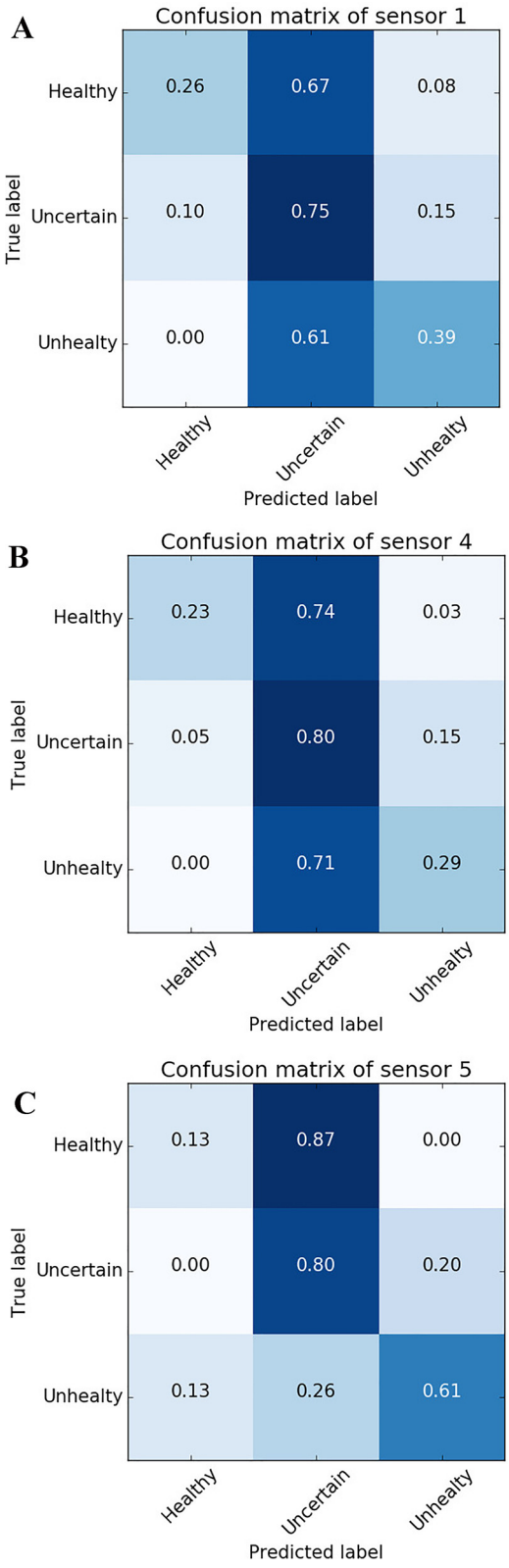

Fig. 11. Confusion matrix of a classifier based on a regression model of (a) sensor 1, (b) sensor 4 and (c) sensor 5.

nanocomposites surface. Moreover, TEM image of the chitosan/PANI nanocomposite shows different size of PANI nanoparticles dispersed in the chitosan matrix causing a longer response times and a lower amplitude response to ammonia [32].

At the same time, Figs. 7 and 8 discover another intriguing feature

Table 3
Diagnostic accuracy (in %) obtained by different classification algorithms and different set of features.

	Features of the resistive curve used to test the algorithm			
Tested algorithm	ΔR	∂R	$\int R$	$\Delta R+\partial R+\int R$
LDA	64	64	67	80
RF	77	77	50	80
SVM	72	77	75	85
MLP	75	78	63	85

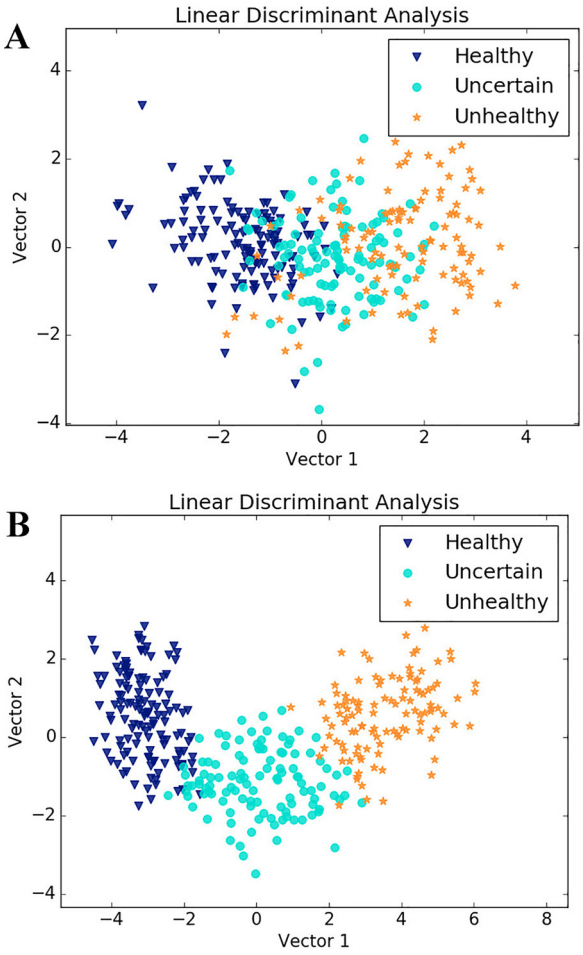

Fig. 12. LDA obtained using (a) the resistance variation of the 11 sensors and (b) using integral and derivative values.

of the sensing behavior of the chitosan/PANI nanocomposite compared to that of other nanocomposites. In particular, its resistance decreases for sensor 1 (with chitosan matrix occluded PANI clusters) and increases for sensors 4 and 5 (with PANI shells located at the surface of core TiO_2 nanoparticles and CNT, respectively).

This specificity of the former suggests that unlike the hybrid core-shell nanocomposites the conducting PANI clusters not only occluded by the chitosan matrix but also can be involved in some physico-chemical interactions with functional groups of chitosan. In particular, these ones can be hydrogen bonding with hydroxyl groups and withdrawing the CSA dopant by highly basic amino groups of chitosan from the doped PANI-CSA clusters, etc. This withdrawing both decreases the chitosan/PANI conductivity (Fig. 7a) and, what is more important, can also change a rate of interaction of this nanocomposite with ammonia as well as affects its selectivity. To clear the latter issue we prolonged the exposure time of the sensors from 1 min till 5 min to allow all PANI

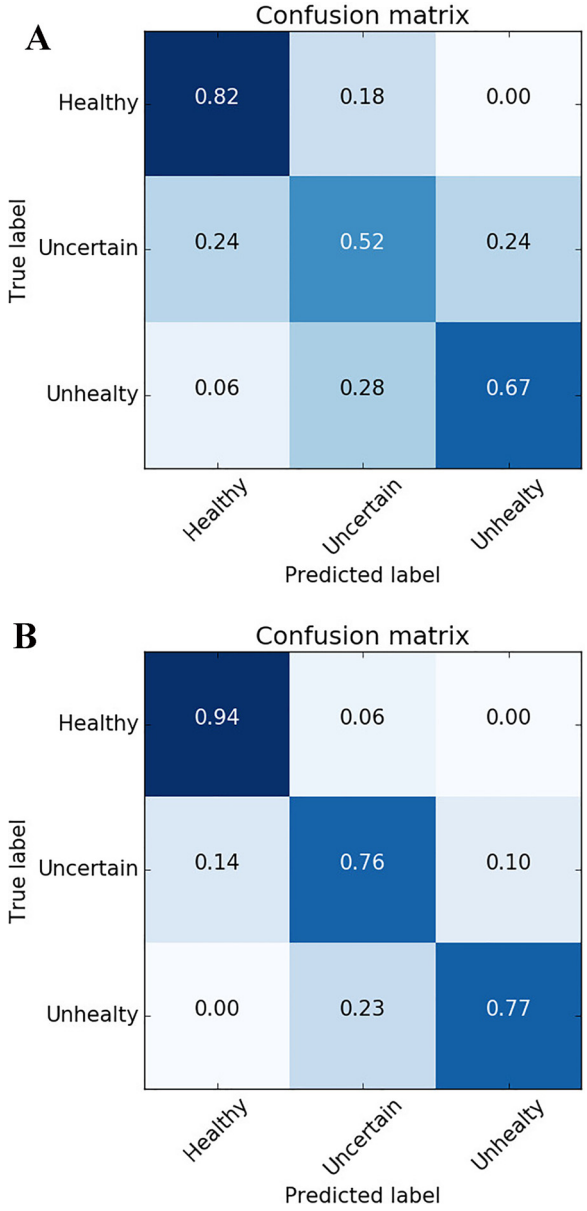

Fig. 13. Confusion matrix of a LDA classifier using (a) the resistance variation of the 11 sensors and (b) using integral and derivative values.

clusters not only in the shells of the hybrid nanocomposites but also in the chitosan matrix to completely interact with the 1 ppm ammonia humidified (50–60 %) air mixture showing a particular phenomenon with chitosan/polyaniline nanocomposite while TiO_2/PANI and CNT/PANI demonstrated the typical resistance growth. Specifically, as one can see in Fig. 10, due to the extension of the exposure, the sensor response of the chitosan/PANI nanocomposite consists of two parts.

The resitance first decreases with the increase of humidity, then increases in a second time in reaction to ammonia. We assign the decrease of the polyaniline resistance to the influence of humidity and the improvement of conditions for interchain charge transfer in polyaniline [40,41] while its increase is naturally due to the interaction with ammonia. In fact, the enhancement of the conductivity of the conducting polymers by the sorption of water molecules is a well-known phenomenon [42,43], which can be explained by the formation of hydrogen bonds between water molecules and either the PANI backbone itself, or with the donor molecules. It has been shown that, in the case of PANI blends, the type of matrix polymer influences on this behavior [44]. It is suggested that the matrix polymers encourage sorption of

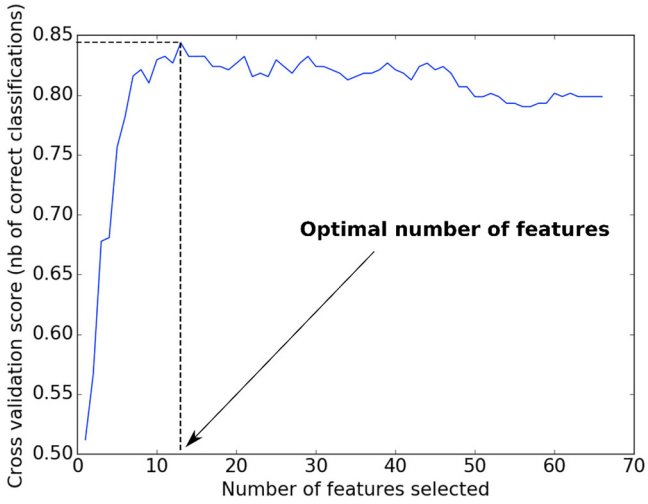

Fig. 14. Accuracy versus number of features selected by RFE for LDA algorithm.

water in the film and allow water molecules to interact with the doped PANI. Probably, this phenomenon strongly prevails for chitosan/PANI nanocomposite when starting the exposure to 1 ppm of ammonia in the air with relative humidity 60% (this humidity roughly corresponds to ~12,000 ppm of water) due to hydrophilicity of chitosan that induces a decrease of the resistance layer. This effect competes with dedoping of the doped PANI by ammonia, which withdraws the dopant (CSA) being in the joint possession of the PANI clusters and amino groups of the chitosan matrix. Existence of these two opposite phenomena results in appearance of the sharp tooth on the curve in Fig. 10 when relative humidity is changed from 50% to 60% and beginning of the prevailing of the nanocomposite interaction with ammonia.

Table 2 summarizes the determined different performances of the synthesized nanocomposite sensors. The selectivity of similar nanocomposites has been investigated and discussed in previous publications, which shown that these materials are quite highly selective to ammonia [18,19,45–47]. The main interfering compound for polyaniline and its nanocomposites sensors for this application is humidity (as discussed above). As for the detection limit, it is not a crucial parameter of the proposed system in the sense that it is expected to measure ammonia in breath, present in relatively large quantities, greater than 500 ppb, but previous studies show that for these nanocomposites, detection limit is below 100 ppb [18,19].

Finally, repeatability of the sensors, characterized by standard deviation, varies from one sensor to another. Standard deviation is higher for chitosan containing sensors than for TiO_2 or CNT containing sensors. Once again high sensitivity to humidity makes chitosan containing sensors less reliable. Other studies achieve better repeatability, as for [25] but the time of measurement is 10 min. This duration is hardly suitable for a handheld diagnosis tool. Standard deviation of TiO_2 sensors are still high because the time of exposure is low, only 60 s A longer time of exposure improves the repeatability. For a classifier based on a regression model of one of these sensors, diagnostic errors are important. This can be visualized using a confusion matrix, Fig. 11. Row gives the class of a tested sample, and column the class predicted by the classifier. The confusion matrix of sensor 1 points out only 26% of healthy sample are correctly classified and 8% classified as an unhealthy sample. Accuracy is calculated by dividing the sum of correctly classified samples by the total sample tested. In these cases, the diagnostic accuracy is 41% for sensor 1, 44% for sensor 4 and 51% for sensor 5.

The following work consists in crossing sensor responses to improve the accuracy of diagnostic.

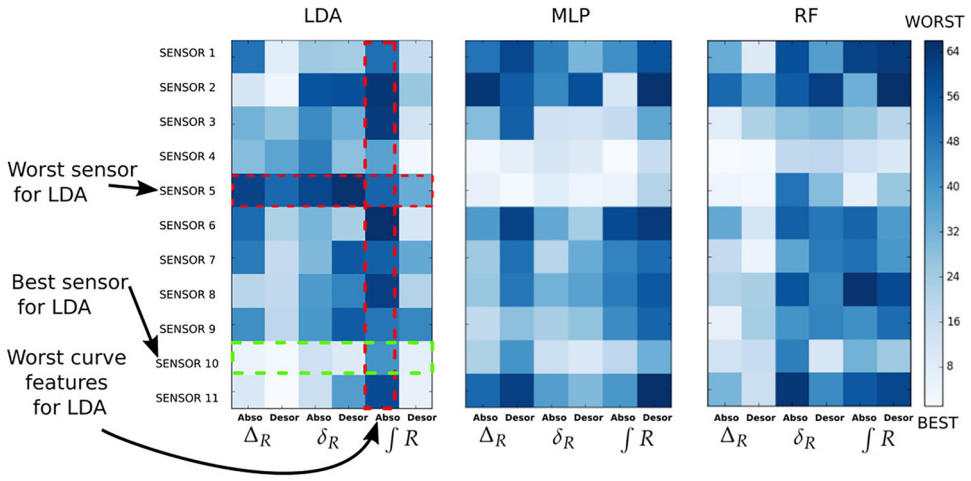

Fig. 15. Illustration of the RFE results. The best features are lighter. Sensor 10 is the more useful for (a) LDA whereas sensors 4 and 5 are the more useful for (b) MLP and (c) RF algorithms.

Table 4
Diagnostic accuracy (in %) obtained by different classification algorithms and different set of features and with RFE.

	Features of the resistive curve used to test the algorithm				
Tested algorithm	ΔR	∂R	$\int R$	$\Delta R + \partial R + \int R$	Selection with RFE
LDA	64	64	67	80	84
RF	77	77	50	80	83
SVM	72	77	75	85	91
MLP	75	78	63	85	87

3.2. Classification results

Each classification algorithm is tested using four sets of features. The first set of feature is the relative resistance variation of each sensor, during the injection and desorption phases. The second set of feature is the maximum derivative. The third one consists of integral values. Finally, a set containing all these features is tested.

Table 3 shows that the different classes are better discriminated when derivative and integer features are added than with the maximum variation only. RF algorithm gives the higher accuracy with the resistance variation only whereas MLP and SVM give the best results with all the features. Accuracy increases by 18% with SVM algorithm if derivative and integer features are added. Fig. 12 shows how the data are projected with LDA algorithm. Classes are clearly better discriminated, 80% of accuracy when the derivatives and the integer parameters are added. By comparison, using only the resistance variation, yields only a 64% accuracy. LDA discriminates better data that are linearly separable that is why SVM and MLP give better accuracy.

Fig. 13 shows that errors occurred only between healthy/uncertain classes, and uncertain/unhealthy. Errors between healthy/unhealthy are possible when resistance variations are the only extracted features. The results are similar with the other tested algorithms.

It is interesting to notice that when the learning dataset and validation dataset are temporally separated, the results are equivalent. That means that sensor responses are indeed reproducible in time.

These results point out that other characteristics extracted from the responses of the sensors clearly improve the accuracy of measurement of polyaniline sensors. The drawback of these results is the number of features that increases the computational time and can increase the risk of overfitting. The next step is then to reduce this number of features. Moreover, by identifying sensors and features extracted from the curves that are the most relevant, improves the future sensor arrays dedicated to the application.

3.3. Improvement with recursive feature elimination

The RFE presented in Section 2.5 is applied. It recursively eliminates the least important feature and calculates the diagnosis accuracy at each iteration. The main information of Fig. 14 is that the maximum accuracy is not obtained with the all available features. In fact, only a small part of them bring the best result: 13 features for LDA, 25 for MLP, 19 for RF and 39 for SVM.

Finally, thanks to RFE, the most important features are extracted from sensors 10 and 11 for LDA and 4 and 5 for MLP and RF, Fig. 15. However, these sensors do not bring enough information to accurately discriminate the samples (accuracy is 65% with these two sensors). Depending on the classifier, the best features are not the same. It is worth pointing out that sensor 5 provides the least information for LDA and the most information for MLP. This is in the sense that MLP can handle non-linear data in the contrast to LDA. Sensor 5, based on CNT, is the one with the worst linearity.

No significant differences between the features extracted during absorption or desorption are evident from these results. Only the integral feature during the absorption phase is useless for LDA, but not for MLP or RF.

This points out that testing several algorithms is an important step to select the right sensor array. Crossing the information of Figs. 14 and 15 yields the best subset.

The classification accuracy improvements brought in by the RFE algorithm are presented in Table 4. With RFE, accuracy increases up to 91% for SVM, 87% for MLP and 84% for LDA while reducing the set of necessary sensors down to 8, 6 and 4 respectively. These values become interesting for a medical application.

4. Conclusions

This paper showed the good effectiveness of using an electronic nose based on the different polyaniline nanocomposites to detect ammonia in a breath simulation. Problems with drift, sensor failure or repeatability make the use of a single sensor less reliable for a measurement system. In particular, the use of a polyaniline nanocomposite sensor network allowed associating the good sensitivity of polyaniline with ammonia while having differentiated responses thanks to different formulations. Thus, diagnostic accuracy of 85% was achieved using SVM algorithm compared to the 44% obtained by basing the classification model on the linear regression of a sensor. A last step of features selection permitted to select the best parameters extracted from the

response curves while improving the accuracy, up to 91%. As electronic nose can be embedded in handheld device, these results pave the way for portable diagnostic systems for kidney disease. Further work will consist of evaluating these results against real breath, which is more complex and variable than that tested.

Declaration of interest

None.

Acknowledgements

This work was supported by a “Future et Ruptures” grant from the “foundation IMT”. The authors acknowledge Dr Lahcen Khouchaf and M D.Betrancourt from IMT Lille Douai for providing SEM and TEM images of the samples.

References

[1] M. Phillips, J. Herrera, S. Krishnan, M. Zain, J. Greenberg, R.N. et Cataneo, Variation in volatile organic compounds in the breath of normal humans, J. Chromatogr. B Biomed. Sci. App 729 (1–2) (1999) 75–88 juin.
[2] M. Phillips, et al., Detection of lung cancer with volatile markers in the breath, Chest J. 123 (6) (2003) 2115–2123.
[3] H. Haick, Y.Y. Broza, P. Mochalski, V. Ruzsanyi, A. et Amann, Assessment, origin, and implementation of breath volatile cancer markers, Chem. Soc. Rev. 43 (5) (2014) 1423–1449.
[4] A. Wehinger, et al., Lung cancer detection by proton transfer reaction mass-spectrometric analysis of human breath gas, Int. J. Mass Spectrom. 265 (1) (2007) 49–59 août.
[5] R. Capuano, et al., The lung cancer breath signature: a comparative analysis of exhaled breath and air sampled from inside the lungs, Sci. Rep. 5 (2015) 16491 nov.
[6] B. Grabowska-Polanowska, et al., Detection of potential chronic kidney disease markers in breath using gas chromatography with mass-spectral detection coupled with thermal desorption method, J. Chromatogr. A 1301 (2013) 179–189 août.
[7] S. Davies, P. Spanel, D. et Smith, Quantitative analysis of ammonia on the breath of patients in end-stage renal failure, Kidney Int. 52 (1) (1997) 223–228 juill.
[8] C. Turner, P. Španěl, D. et Smith, A longitudinal study of ammonia, acetone and propanol in the exhaled breath of 30 subjects using selected ion flow tube mass spectrometry, SIFT-MS, Physiol. Meas. 27 (4) (2006) 321.
[9] Global, regional, and national incidence, prevalence, and years lived with disability for 310 diseases and injuries, 1990–2015: a systematic analysis for the Global Burden of Disease Study 2015, Lancet Lond. Engl. 388 (10053) (2016) 1545–1602 oct.
[10] P.B. Bach, et al., Benefits and harms of CT screening for lung Cancer: a systematic review, JAMA J. Am. Med. Assoc. 307 (22) (2012) 2418–2429 juin.
[11] S.-J. Kim, S.-J. Choi, J.-S. Jang, H.-J. Cho, I.-D. et Kim, Innovative nanosensor for disease diagnosis, Acc. Chem. Res. 50 (7) (2017) 1587–1596 juill.
[12] J.-W. Yoon, J.-H. et Lee, Toward breath analysis on a chip for disease diagnosis using semiconductor-based chemiresistors: recent progress and future perspectives, Lab Chip 17 (21) (2017) 3537–3557 oct.
[13] M. Rodahl, F. Höök, A. Krozer, P. Brzezinski, B. et Kasemo, Quartz crystal microbalance setup for frequency and Q-factor measurements in gaseous and liquid environments, Rev. Sci. Instrum. 66 (7) (1995) 3924–3930 juill.
[14] M. Kikuchi, K. Omori, S. et Shiratori, Quartz crystal microbalance (QCM) sensor for ammonia gas using clay/polyelectrolyte layer-by-layer self-assembly film, Proc. IEEE Sens. 2 (2004) (2004) 718–721.
[15] K. Arshak, E. Moore, G.M. Lyons, J. Harris, S. et Clifford, A review of gas sensors employed in electronic nose applications, Sens. Rev. 24 (2) (2004) 181–198 juin.
[16] P. Gouma, K. Kalyanasundaram, X. Yun, M. Stanacevic, L. et Wang, Nanosensor and breath analyzer for Ammonia detection in exhaled human breath, IEEE Sens. J. 10 (1) (2010) 49–53 janv.
[17] J.L. Wojkiewicz, et al., Nanostructured polyaniline-based composites for ppb range ammonia sensing, Sens. Actuators B Chem. 160 (1) (2011) 1394–1403 déc.
[18] S. Mikhaylov, et al., Ammonia/amine electronic gas sensors based on hybrid polyaniline–TiO2 nanocomposites. The effects of titania and the surface active doping acid, RSC Adv. 5 (26) (2015) 20218–20226 févr.
[19] T. Mérian, N. Redon, Z. Zujovic, D. Stanisavljev, J.L. Wojkiewicz, M. et Gizdavic-Nikolaidis, Ultra sensitive ammonia sensors based on microwave synthesized nanofibrillar polyanilines, Sens. Actuators B Chem. 203 (2014) 626–634 nov.
[20] S. Mikhaylov, Synthesis and Investigation of Nanostructured Conducting Polymers Based Nanocomposites for Ammonia and Amines, Université de Lille, IMT Lille Douai and Institute of Bioorganic Chemistry and Petrochemistry, Kiev, 2017.
[21] J. Gong, Y. Li, Z. Hu, Z. Zhou, Y. et Deng, Ultrasensitive NH3 gas sensor from polyaniline nanograin enchased TiO2 fibers, J. Phys. Chem. C 114 (21) (2010) 9970–9974 juin.
[22] J.N. Coleman, et al., Physical doping of a conjugated polymer with carbon nanotubes, Synth. Met. 102 (1) (1999) 1174–1175 juin.
[23] J.N. Coleman, et al., Percolation-dominated conductivity in a conjugated-polymer-carbon-nanotube composite, Phys. Rev. B 58 (12) (1998) R7492–R7495 sept.
[24] M. Cochet, et al., Synthesis of a new polyaniline/nanotube composite: “in-situ” polymerisation and charge transfer through site-selective interaction, Chem. Commun. 0 (16) (2001) 1450–1451 janv.
[25] T. Hibbard, K. Crowley, A.J. et Killard, Direct measurement of ammonia in simulated human breath using an inkjet-printed polyaniline nanoparticle sensor, Anal. Chim. Acta 779 (2013) 56–63 mai.
[26] M.C. Santos, A.G.C. Bianchi, D.M. Ushizima, F.J. Pavinatto, R.F. et Bianchi, Ammonia gas sensor based on the frequency-dependent impedance characteristics of ultrathin polyaniline films, Sens. Actuators Phys. 253 (2017) 156–164 janv.
[27] H. Haick, Chemical sensors based on molecularly modified metallic nanoparticles, *ResearchGate* 40 (23) (2007) 7173–7186 déc.
[28] G. Magna, F. Mosciano, E. Martinelli, C. et Di Natale, Unsupervised on-line selection of training features for a robust classification with drifting and faulty gas sensors, Sens. Actuators B Chem. 258 (2018) 1242–1251 avr.
[29] T. Sen, S. Mishra, N.G. et Shimpi, Synthesis and sensing applications of polyaniline nanocomposites: a review, RSC Adv. 6 (48) (2016) 42196–42222 avr.
[30] N.R. Tanguy, M. Thompson, N. et Yan, A review on advances in application of polyaniline for ammonia detection, Sens. Actuators B Chem. 257 (2018) 1044–1064 mars.
[31] GMP chitosan, Heppe Medical chitosan, pharma grade chitosan, pure chitosan, chitosan derivatives, GMP, Qualität, Heppe Medical Chitosan.
[32] J.L. Wojkiewicz, et al., Hybrid and bio nanocomposites for ultrasensitive Ammonia sensors, Proceedings 1 (4) (2017) 407 août.
[33] J.L. Wojkiewicz, A.A. Pud, V.N. Bliznyuk, T. Lasri, Y.V. et Noskov, Synthesis of polyaniline/carbon Nanotubes Nanocomposites and Their Sensing Properties to Methylamine, (2012), p. 3.
[34] S.M. Scott, D. James, Z. et Ali, Data analysis for electronic nose systems, Microchim. Acta 156 (3–4) (2006) 183–207 déc.
[35] J.L. Wojkiewicz et, Nanostructured conducting polymers: new materials for high performance gas sensors, BIT’s 6th Annu. World Congr. Nanosci. Nanotechnol. (2016), pp. 475–481 Book abstract, oct.
[36] T. Eklöv, P. Mårtensson, I. et Lundström, Selection of variables for interpreting multivariate gas sensor data, Anal. Chim. Acta 381 (2) (1999) 221–232 févr..
[37] J.H. Leopold, et al., Comparison of classification methods in breath analysis by electronic nose, J. Breath Res. 9 (4) (2015) 046002 déc.
[38] C. Cortes, V. et Vapnik, Support-vector networks, Mach. Learn. 20 (3) (1995) 273–297 sept.
[39] L. Breiman, Random forests, Mach. Learn. 45 (1) (2001) 5–32 oct.
[40] F. Pedregosa et al., Scikit-learn: Machine Learning in Python, Mach. Learn. PYTHON, 6.
[41] A.T. Ramaprasad, V. et Rao, Chitin–polyaniline blend as humidity sensor, Sens. Actuators B Chem. 148 (1) (2010) 117–125 juin.
[42] S.T. McGovern, G.M. Spinks, G.G. et Wallace, Micro-humidity sensors based on a processable polyaniline blend, Sens. Actuators B Chem. 107 (2) (2005) 657–665 juin.
[43] M. Matsuguchi, J. Io, G. Sugiyama, Y. et Sakai, Effect of NH3 gas on the electrical conductivity of polyaniline blend films, Synth. Met. 128 (1) (2002) 15–19 avr.
[44] M. Matsuguchi, A. Okamoto, Y. et Sakai, Effect of humidity on NH3 gas sensitivity of polyaniline blend films, Sens. Actuators B Chem. 94 (1) (2003) 46–52 août.
[45] L. Kumar, I. Rawal, A. Kaur, S. et Annapoorni, Flexible room temperature ammonia sensor based on polyaniline, Sens. Actuators B Chem. 240 (2017) 408–416 mars.
[46] Lina Xuea, Wen et Wanga, Flexible polyaniline/carbon nanotube nanocomposite film-based electronic gas sensors, Sens. Actuators B Chem. 244 (2017) 47–53.
[47] S. Abdulla, T.L. Mathew, B. et Pullithadathil, Highly sensitive, room temperature gas sensor based on polyaniline-multiwalled carbon nanotubes (PANI/MWCNTs) nanocomposite for trace-level ammonia detection, Sens. Actuators B Chem. 221 (2015) 1523–1534 déc.

Paul Le Maout received the M.Sc. degree from Université de Bretagne Occidentale in Brest and the Engineer’s Degree from Ecole Nationale d’Ingénieurs de Brest, Brittany, France in 2016. He is a Ph.D student at IMT Atlantique in Brest and his current research are electronic nose for disease diagnosis. His interests include conducting polymer sensor array, impedance measurement and classification algorithms.

Jean-Luc Wojkiewicz is HDR in physical sciences (2012) and PhD in material science (1984), he is elected as Professor in September 2013 and gives lectures in general physics at Institut Mines Telecom Lille Douai. He created the conducting polymer laboratory in 1992 and joined the Atmospheric Science and Environment Engineering in « Institut Mines Telecom ». His research interests are focused on the synthesis, electronic, electromagnetic studies of nanostructured conducting polymers. In the frame of international collaborations, new electronic organic gas sensors were optimized to get extremely low detection threshold for atmospheric pollutants detection. Now, he is working on the development of new nanostructured materials based on polyaniline/Graphene nanocomposites to detect Volatile Organic Compounds at extremely low concentration which can be integrated in an e-nose. These material performances are used for medical diagnosis to detect diseases (cancer, renal failure.) by breath analysis. Other applications are also investigated as flexible antennas, electromagnetic shielding or radar absorbing materials.

Nathalie Redon have a Ph.D. in electronic, works on micro-sensors for air quality applications in the Research Department of Atmospheric Sciences at IMT Lille Douai. She works on one hand on the development of electronic sensitive surfaces for pollutants detection and quantification of specific gases or particles involved in indoor air or in ambient air. The sensitive materials synthesized are based on intrinsic conductive nanocomposites, with fiber or core-shell structures based on polyaniline-typ polymers.

Pollutants specifically targeted are ammonia, amines, formaldehyde, hydrogen sulfide, and ammonium nitrate. On the other hand, she studies how the use of pollutants micro-sensor networks can help scientists to assess semi-quantitative pollution qualification for indoor/outdoor air applications (eg quality index of air pollution, determination and monitoring of the efficiency of air treatment processes) or health diagnosis by breath analysis. In this context, she explores the potential of multivariate analysis, including data processing by neural or bayesian networks analyses, to identify odors or air or breath pollution signatures. Finally, as a member of the LCSQA (Central Laboratory for Air Quality Monitoring), Nathalie REDON is in charge of the development and implementation of metrological evaluation protocols for micro-sensors for the indicative measurement of regulated pollutants (gases and particles).

Cyril Lahuec received the B.Sc. (Hon.) degree from the University of Central Lancashire, U.K., in 1993, his M.Eng. (mode A, by research) and Ph.D. degrees from Cork Institute of Technology, Ireland, in 1999 and 2002, respectively. In 2012, he received the Research Habilitation from the University of South Brittany, Brittany. It is the highest French university degree passed after a few years of active research and student supervisions. He was with Parthus Technologies (now Ceva) Cork for his Ph.D. work and then as a Consultant. He joined the Department of Electronic Engineering of TELECOM Bretagne, Brest, France, as a full-time Lecturer in 2002. He was a Visiting Scholar at the University of Edinburgh for 4 months in 2011. His research interests are in frequency synthesis, analogue IC design, channel decoding, and biomedical applications.

Fabrice Seguin received the Ph.D. degree from the Universite Bordeaux 1, France, in 2001. His doctoral research concerned the current mode design of high-speed current-conveyors and applications in RF circuits. In 2002, he joined the Electronic Engineering Department of Telecom Bretagne, Brest, France, as a full-time lecturer. At PRACOM, (Pôle de Recherche Avancée en Communications) he is currently involved with design issues of analogue channel decoders and related topics.

Laurent Dupont received his engineering degree from Ecole Nationale Superieure de Chimie et Physique de Bordeaux in 1986. He received a doctorate from the University of Bordeaux I in 1990 in physics of ferroelectric liquid crystals. Then, he joined the optics Department of TELECOM BRETAGNE in 1991, where he was in charge of the liquid crystal technologies lab devoted to the optical applications of liquid crystal materials. Since 2000 he has worked on various aspects of polarization issues in the telecom transmission systems and in particular on the polarization mode dispersion in optical fibers. He involved RNRT COPOLDYN project for the realization of a polarization controller based on Liquid Crystal. He is coordinator of the project ANR Lambda-Access on tuneable VCSEL sources and he is partner in the project Select-Access for the realization of polarization splitters for fring resonator filters in WDM networks. and polarization insensitive. He currently involve in the ANR P3N project NASTAROD about electrooptic effect of clays suspension. He has supervised more than 12 PhD students and he wroted or co-authored over 80 publications in journals, primarily in the field of Liquid crystal technology. He is also the holder of nine patents. He participated to the creation of 3 companies: Optogone, Lixy and E3S.

Sergei Mikhaylov completed his PhD in frames of the joint project between IMT Lille-Douai and IBCP NAS of Ukraine entitled “Synthesis and investigation of nanostructured conducting polymers based nanocomposites for ammonia and amines detection”. His research interests include conducting polymers, fabrication of chemical and biosensors, functional nanomaterials.

Yuriy V. Noskov currently is a Research Fellow in the Department of Chemistry of Functional Materials of the Institute of Bioorganic Chemistry and Petrochemistry of NAS of Ukraine. He graduated from Kiev Taras Shevchenko National University, Chemical Department (2004). He received a PhD degree in 2010 in Macromolecular Chemistry, at Chemistry Department of Kiev Taras Shevchenko National University (Ukraine). His scientific interests are focused on synthesis of conjugated polymers and their multi-functional hybrid nanocomposites, nanoparticles and their applications as sensor materials, in solar cells drug delivery systems, etc.

Nikolay A. Ogurtsov studied chemistry at the Lomonosov Moscow State University. In 1991, he received his Ph.D. in chemistry at Pisarzhevsky Institute of Physical Chemistry of the National Academy of Sciences of Ukraine (NASU), Kiev. Since 2001, he is a Senior Researcher at the Institute of Bioorganic Chemistry and Petrochemistry of NASU. His current research interests focus on synthesis of nanocomposites based on conducting polymers, the structure–property relationship of such materials.

Alexander A. Pud since 2009 is the Head of the Department of Chemistry of Functional Materials of the Institute of Bioorganic Chemistry and Petrochemistry of NAS of Ukraine. He graduated from Kiev Polytechnic Institute, Department of Electrochemical Productions Technology (1979). In 1985 and 2004 he received his PhD degree and Dr. Sci. (HDR) in Polymer Science, at Chemistry Department of Kiev State University, Ukraine respectively. In 1999 he was awarded with Kiprianov Prize of National Academy of Sciences of Ukraine for the cycle of works performed jointly with Prof. Dr. G.S. Shapoval “Electrochemically initiated transformations of macromolecules”. In 2011 he became the Professor in Physical Chemistry. His research interests currently are in fields of chemical and electrochemical formation, properties and functioning of intrinsically conducting polymer (ICP) structures in dispersion and solid-phase media; synthesis, properties and applications of multifunctional host-guest (core-shell) hybrid (nano)composites of ICP (e.g. polyaniline, polythiophene and their derivatives) with both polymers of other nature and inorganic nanoparticles (semiconductor, dielectric, magnetic etc.).